Int. J. Heat Mass Transfer. Vol. 31, No. 11, pp. 2261–2272, 1988
Printed in Great Britain

0017–9310/88 $3.00 + 0.00

Spectral correlated and non-correlated radiative transfer in a finite axisymmetric system containing an absorbing and emitting real gas–particle mixture

L. ZHANG, A. SOUFIANI and J. TAINE

Laboratoire d'Energétique Moléculaire et Macroscopique, Combustion,
Ecole Centrale des Arts et Manufactures, 92295 Châtenay-Malabry Cedex, France

(*Received* 10 *December* 1987 *and in final form* 22 *February* 1988)

Abstract—Radiative transfer in a finite axisymmetric enclosure is investigated for a non-isothermal, inhomogeneous, absorbing, emitting but non-scattering gas–particle mixture. A random statistical narrow band model and the Curtis–Godson approximation are used to calculate the real gas radiative properties. High resolution spectral correlations between the transmissivities of homogeneous and isothermal discretization column elements are treated by an ellipse correlation model which is validated. A discrete-direction method is applied to solve the geometrical part of the radiative transfer problem. Applications to planar and finite axisymmetric geometries show that spectral correlations significantly modify, typically 30–50%, the radiative flux and radiative dissipation in practical systems. Non-correlated models may lead to inaccurate qualitative predictions (e.g. the radiative flux sign may be reversed).

1. INTRODUCTION

RADIATIVE transfer must be accurately modelled in practical systems such as combustion chambers, boilers and furnaces, gas turbine combustors, rocket and aircraft engines, etc. Many of these systems can be considered as finite-length axisymmetric enclosures. Most of the previous studies are related to one-dimensional infinite cylindrical geometries (see ref. [1] for a literature survey). The works related to finite axisymmetric enclosures [2, 3] or tri-dimensional geometries [4] use generally gray gas models, which are not satisfactory except when the diffusion by large size particles is predominant. Other works use the exponential wide band model due to Edwards and co-workers [5–8] for cylindrical systems [8, 9]. The exponential wide band model accounts for discrete absorption bands and spectral correlations resulting from the high resolution structure. However, the spectral discretization used in this model is too wide and does not take into account the low resolution correlations between intensities and transmissivities [10]; on the other hand, the case of partially reflecting walls cannot be correctly modelled with this approach [6]. These two disadvantages are avoided when a statistical narrow band model is used in radiative transfer calculations [10–12]. In other works [13, 14], the spectral difficulty has been treated by using a simplified approach in the case of an elementary column; total transmittance data were calculated from a statistical narrow band model and characteristic temperature and pressure conditions of the column [13, 14].

We apply in the present study a random statistical narrow band (RSNB) model [15] and the Curtis–Godson (CG) approximation [16] to calculate gas radiative properties. These properties are used to solve numerically the radiative transfer problem in a finite axisymmetric enclosure containing an inhomogeneous non-isothermal and non-scattering H_2O–CO_2–CO–air–particle mixture. The geometrical part of the radiative transfer problem is treated with a discrete-direction method. An exact correlated calculation of intensities at all the medium points and for all the directions is CPU time and storage consuming; it is easier to compute, step by step, the intensity field while not accounting for spectral correlations between column elements of the spatial discretization. The purposes of this paper are: (i) to investigate the influence of these correlations; (ii) to elaborate and validate an approximated ellipse correlation (EC) model based on an exact correlated calculation for some discrete directions. The correlated radiative intensity is obtained from the product of the corresponding non-correlated intensity and a corrective factor given by the EC model.

The basic formulation of the problem, the modelling of the mixture radiative properties, and the choice of spectral, spatial and directional discretizations are exposed in Sections 2.1, 2.2 and 2.3, respectively. The ellipse correlation model is developed in Section 2.3.3. Results from this model are compared with those from an exact calculation for a planar medium in Section 3.1, and to those from a non-correlated model for a finite cylindrical system in Section 3.2.

NOMENCLATURE

a	coefficient related to wall leaving intensity contributions
C	correlation coefficient
E	distance between the walls in planar geometry
$\mathbf{e}$	unit vector along a coordinate axis
f	geometrical coefficient
f_v	particle volume fraction
G	medium emission contribution
I, I_v	radiative intensity
I_b	blackbody intensity
J, K, M	medium grid points
L	cylinder length
l	element column length
N_r	radial discretization total number
N_y	axial discretization total number
N_θ	θ discretization total number
N_Ω	solid angle discretization total number
$\mathbf{n}$	unitary normal vector pointed outside the wall
p	pressure
$P(M)$	radiative dissipation
P_k	cut plane parallel to the system axis
q_i	incident radiative flux
q_w	wall radiative flux
R	largest radius of an axisymmetric system
r	radial coordinate
$r_w(y)$	local radius of an axisymmetric enclosure
S	wall grid point
T	temperature
U	optical path length
$\mathbf{u}$	unitary vector of an elementary solid angle
x_i	molar fraction of species i
y	axial coordinate
z	transverse coordinate in the plane P_k.

Greek symbols

$\bar{\beta}$	mean line-width to spacing ratio
$\bar{\gamma}$	mean half-width of the absorption lines inside $\Delta\nu$
$\bar{\delta}$	equivalent line spacing
ε	emissivity
θ	angle in a plane P_k
ν	wave number
$\Delta\nu$	spectral range
τ	transmissivity
Φ	angle characterizing the plane P_k
Ω	solid angle.

Subscripts

i	wall incident quantity
k	radial discretization
l	wall leaving quantity
m	θ discretization in the plane P_k
s	related to a wall point S
y	component in the y-direction
z	component in the z-direction
ν	spectral quantity.

Superscripts

$\bar{}$	properties averaged over the spectral range $\Delta\nu$
$*$	non-correlated quantities.

Index

i	discretization over the y-direction
j	discretization over the z-direction.

2. ANALYSIS

2.1. *Basic formulation*

The spectrum is divided into a number of $\Delta\nu$ wide finite intervals inside which the blackbody intensity is constant. We consider, in a first step, quantities averaged over a spectral range $\Delta\nu$; e.g. the radiative intensity $\bar{I}_\nu(M, \mathbf{u})$ at a point M in the direction characterized by the unit vector $\mathbf{u}$ is

$$\bar{I}_\nu(M, \mathbf{u}) = \frac{1}{\Delta\nu}\int_{\Delta\nu} I_\nu(M, \mathbf{u})\, d\nu' \qquad (1)$$

where $I_\nu(M, \mathbf{u})$ is the spectral radiative intensity at the same point in the same direction. The radiative intensity leaving an isothermal and homogeneous column element of length l, at temperature T, containing an absorbing, emitting but non-scattering gas–particle mixture is given by

$$\bar{I}_\nu(l, \mathbf{u}) = \overline{\tau_\nu I_\nu}(0, \mathbf{u}) + (1 - \bar{\tau}_\nu) I_{b\nu}(T) \qquad (2)$$

where $I_\nu(0, \mathbf{u})$ and $I_{b\nu}(T)$ are respectively the spectral intensity at the entrance of the column and the spectral blackbody intensity at temperature T; τ_ν is the spectral transmissivity of the column. Averaged quantities $\bar{\tau}_\nu$ and $\overline{\tau_\nu I_\nu}(0, \mathbf{u})$ are obtained from integrations similar to equation (1). The averaged product $\overline{\tau_\nu I_\nu}(0, \mathbf{u})$ is not equal to the product $\bar{\tau}_\nu \bar{I}_\nu(0, \mathbf{u})$ because τ_ν and $I_\nu(0, \mathbf{u})$ are spectrally correlated. This correlation phenomenon is due to the high resolution structure of the spectrum; e.g. a few hundred resolved lines may appear in a 25 cm^{-1} wide range of an absorption band of CO_2 or H_2O.

For given distributions of temperature T, pressure P, molar fraction x_i of all the gas species and particle characteristic parameters, the radiative flux $q_w(S)$ at any point S of a diffuse wall and the radiative dissipation $P(M)$ at any point M of the medium can be calculated from

$$P(M) = \sum_{\text{spectrum}} \left\{ -\text{div}\left[\int_{4\pi} \bar{I}_\nu(M, \mathbf{u})\mathbf{u}\, d\Omega \right] \right\} \Delta\nu \quad (3)$$

and

$$q_w(S) = \sum_{\text{spectrum}} \varepsilon_\nu(S)\{q_{i\nu}(S) - \pi I_{b\nu}[T(S)]\}\Delta\nu \quad (4)$$

where $\varepsilon_\nu(S)$ and $q_{i\nu}(S)$ designate respectively the wall emissivity and incident radiative flux per unit area at wall point S; the latter is given by

$$q_{i\nu}(S) = \int \overline{I_{i\nu}}(S, \mathbf{u})\mathbf{u}\cdot\mathbf{n}\, d\Omega \quad (\mathbf{u}\cdot\mathbf{n} \geqslant 0). \quad (5)$$

In this equation, $\overline{I_{i\nu}}(S, \mathbf{u})$ is the incident intensity at point S from the direction $\mathbf{u}$ and $\mathbf{n}$ the unitary normal vector pointed outside the wall. In the case of diffuse walls, the leaving intensity $\overline{I_{i\nu}}(S, \mathbf{u})$ at the wall point S is not dependent on the direction $\mathbf{u}$ and is written as

$$\overline{I_{i\nu}}(S) = \varepsilon_\nu(S) I_{b\nu}[T(S)] + \frac{1-\varepsilon_\nu(S)}{\pi} q_{i\nu}(S). \quad (6)$$

Equation (2) enables a step-by-step calculation of the intensity at any point from the wall leaving intensities $\overline{I_{i\nu}}(S)$. Therefore, the incident radiative flux $q_{i\nu}(S)$ is a function of the leaving intensities at the wall points. A linear equation system, in which the unknown quantities are $q_{i\nu}(S)$ (or $\overline{I_{i\nu}}$), is thus obtained. The range of this system is equal to the number of wall discretization points. When this system is solved, the radiative flux $q_w(S)$ and the radiative dissipation $P(M)$ are obtained from equations (2)–(4).

2.2. *Radiative properties of the mixture*

The main difficulty in real gas radiative transfer treatment is to calculate the spectral correlated terms which appear in equation (2). A gray gas model, using a wave number-independent absorption coefficient, has no physical meaning. The wide-band model, due to Edwards and co-workers [5, 6], and derivative models such as that of Tien and Lowder [7], take into account spectral correlations but present two disadvantages: (i) reflexion by the wall cannot be correctly taken into account; (ii) the spectral discretization is too wide and leads to errors in the radiative flux distribution for an intermediate optical length medium. Investigations about different radiative band models have been carried out in previous publications associated with one-dimensional radiative transfer coupled with conduction [11] or with convection [10, 12]. The most accurate temperature and flux distributions are obtained with the RSNB model, due to Mayer and Goody [15], and an exponential-tailed-inverse line-strength distribution [17]. The transmissivity of an elementary homogeneous and isothermal column of length l due to gas species i, averaged over the spectral range $\Delta\nu$, is then given by

$$\bar{\tau}_\nu^i = \exp\left[-\frac{\bar{\beta}}{\pi}\left(\sqrt{\left(1 + \frac{2\pi x_i P l \bar{k}}{\bar{\beta}} \right)} - 1 \right) \right] \quad (7)$$

where x_i and P are respectively the molar fraction of the absorbing species i and total pressure; $\bar{k}$ and $\bar{\beta} = 2\pi\bar{\gamma}/\bar{\delta}$ are the band model parameters which take into account the spectral structure of the gas. Parameters $\bar{k}$ and $1/\bar{\delta}$ may be generated either from experimental spectra (e.g. ref. [18] for H_2O) or from a line by line calculation [11, 19–21] at different temperatures. In the present study we use the previously published parameters $\bar{k}$ and $1/\bar{\delta}$ [11, 21], associated with the mean half-width $\bar{\gamma}$ given by

$$\bar{\gamma}_{H_2O} = 0.066 \frac{P}{P_s} \left\{ 7.0 x_{H_2O} \frac{T_s}{T} + [1.2(x_{H_2O} + x_{N_2}) + 0.8 x_{O_2} + 1.6 x_{CO_2}] \sqrt{\left(\frac{T_s}{T} \right)} \right\} \quad (8)$$

and

$$\bar{\gamma}_{CO_2} = \frac{P}{P_s}\left(\frac{T_s}{T} \right)^{0.7} \times [0.07 x_{CO_2} + 0.058(x_{N_2} + x_{O_2}) + 0.15 x_{H_2O}] \quad (9)$$

where P_s and T_s designate standard pressure and temperature (1 atm, 296 K).

For a non-isothermal and inhomogeneous column, the CG approximation [16, 22] leads to accurate results if pressure gradients are not too large [23]. The basic idea of this approach consists in the transformation of such a column into an equivalent isothermal and homogeneous one. Effective band model parameters $\bar{k}_e$ and $\bar{\beta}_e$ are introduced by averaging $\bar{k}$ and $\bar{\beta}$ over the optical path U of the column

$$U(l) = \int_0^l P(M) x_i(M)\, dl \quad (10)$$

$$\bar{k}_e = \frac{1}{U(l)} \int_0^l P(M) x_i(M) \bar{k}(M)\, dl \quad (11)$$

$$\bar{\beta}_e = \frac{1}{\bar{k}_e U(l)} \int_0^l P(M) x_i(M) \bar{k}(M) \bar{\beta}(M)\, dl. \quad (12)$$

The transmissivity of this equivalent column is then calculated from equation (7).

When absorption by different gas species occurs inside the same spectral range $\Delta\nu$, these phenomena can be considered as not correlated [15]; the transmissivity $\bar{\tau}_\nu^g$ of the mixture column is then the product of those related to each species.

We consider only particles of characteristic size smaller than the radiation dominant wavelength; the particle spectral absorption coefficient is then given by [24]

$$K_\nu^p = 36\pi f_v \nu \frac{n\chi}{[n^2 - (n\chi)^2 + 2] + (2n\chi)^2} \quad (13)$$

where f_v is the particle volume fraction, n and χ are

the real and imaginary parts of the refractive index, respectively. As K_ν^p has no fine structure inside $\Delta\nu$, absorption by particles is not correlated with that by the gas; the transmissivity $\bar{\tau}_\nu$ averaged over $\Delta\nu$, of a column element is the product of the transmissivities $\bar{\tau}_\nu^g$ of the gas and $\bar{\tau}_\nu^p$ of the particles.

2.3. *Radiative transfer model*

Temperature, concentration and pressure fields, and particle characteristics are supposed to be known. The wall emissivity is assumed to be diffuse but not necessarily gray. The wall temperature distribution is also given.

In order to compute the radiative flux and dissipation inside $\Delta\nu$, two discretizations are necessary: (i) a spatial discretization, i.e. the choice of the grid points where the radiative intensities are calculated; (ii) a directional discretization, i.e. the definition of elementary solid angles $\Delta\Omega$ around discrete directions $\mathbf{u}$. The spatial discretization is not consistent with the directional one; the axis of an elementary solid angle, which passes through a grid point, generally does not pass through another grid point. It is impracticable to carry out an exact calculation of correlated intensities at all the grid points and for all the discretized directions; although this calculation is possible for a one-dimensional planar geometry [10, 11].

The method proposed here consists in: (i) defining optimal spatial and directional discretizations (Section 2.3.1); (ii) carrying out a non-correlated calculation of the intensities at each grid point in all the discretized directions (Section 2.3.2); (iii) taking into account the spectral correlations at all the grid points and in all the directions by use of an ellipse correlation model (Section 2.3.3); this model is based on exact correlated calculations in particular directions. The accuracy of this corrective model will be discussed in the same section.

2.3.1. *Spatial and directional discretizations.* An axisymmetric finite enclosure of length L is defined by

$$r = r_w(y) \quad (0 \leqslant y \leqslant L) \tag{14}$$

where r and y are respectively the radial and axial coordinates, and r_w designates the radius of a lateral wall.

The medium grid curves are the circles (y_i, r_k) which are the intersections of N_r coaxial cylinders called r_k, and a series of planes called y_i $(i = 1, 2, \ldots, N_y)$, normal to the system axis. The radii of the coaxial cylinders are r_k $(k = 0, 1, 2, \ldots, N_r)$ with $r_0 = 0$ and $r_{N_r} = R$, radius of the largest cylinder. The wall grid curves are the intersections between the walls and the N_y planes y_i or the N_r coaxial cylinders r_k.

The directional discretization consists in dividing, at each point M of the medium, the space into N_Ω elementary solid angles quoted $\Delta\Omega_l$ $(l = 1, 2, \ldots, N_\Omega)$ and characterized by a unit vector $\mathbf{u}$. If N_Ω is large enough, the radiative flux vector is written as

$$\mathbf{q}_\nu(M) = \int_{4\pi} \bar{I}_\nu(M, \mathbf{u})\mathbf{u}\, d\Omega = \sum_{l=1}^{N_\Omega} \int_{\Delta\Omega_l} \bar{I}_\nu(M, \mathbf{u})\mathbf{u}\, d\Omega \approx \sum_{l=1}^{N_\Omega} \bar{I}_\nu(M, \mathbf{u}) \int_{\Delta\Omega_l} \mathbf{u}\, d\Omega. \tag{15}$$

From any wall point S_0 of the grid circle (y_i, R), we define N_r planes tangent to the coaxial cylinders r_k $(k = 0, 1, 2, \ldots, N_r - 1)$ quoted $P_k(R)$ (Fig. 1). The angle $\Phi_k(R)$ between planes $P_0(R)$ and $P_k(R)$ is given by

$$\Phi_k(R) = \sin^{-1}(r_k/R) \quad (k = 0, 1, \ldots, N_r - 1). \tag{16}$$

N_r wedges, having the same edge S_0y (Fig. 1) and divided into two equal parts by the plane $P_k(R)$, are introduced. The angles $\Delta\Phi_k(R)$ of these wedges are given by the recurrence relations

$$\Delta\Phi_0(R) = \Phi_1(R)$$

$$\Delta\Phi_k(R) = 2[\Phi_k(R) - \Phi_{(k-1)}(R)] - \Delta\Phi_{(k-1)}(R), \quad k = 1, 2, \ldots, N_r - 2$$

$$\Delta\Phi_k(R) = \pi/2 - [\Phi_{(k-1)}(R) + 0.5\Delta\Phi_{(k-1)}(R)], \quad k = N_r - 1. \tag{17}$$

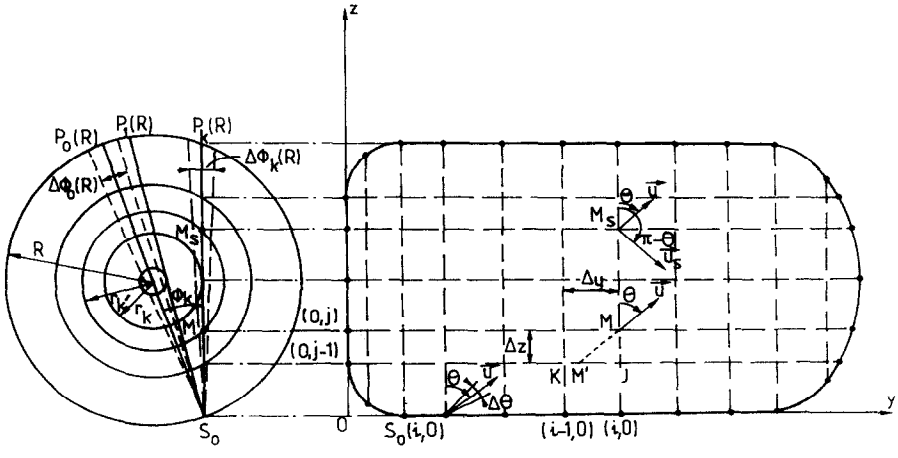

FIG. 1. Directional discretization of an axisymmetric system and mesh network on the plane $P_k(R)$.

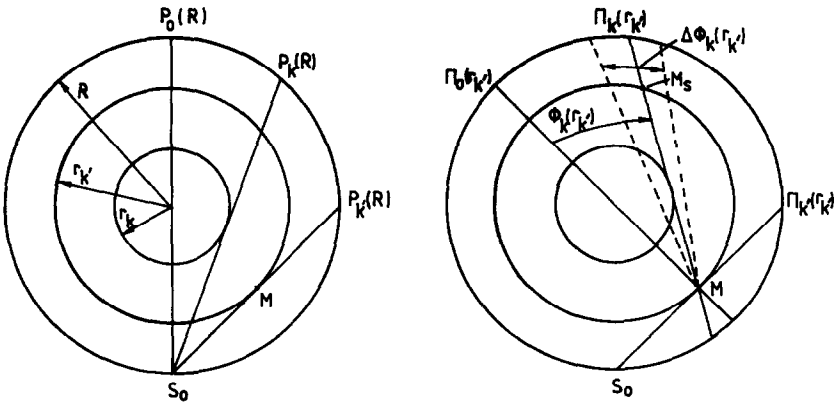

FIG. 2. Discretization of angle Φ for the grid points on the cylinder $r_{k'} < R$. (Radiation fields in the planes $\Pi_k(r_{k'})$ and $P_k(R)$ are identical.)

A y–z coordinate system is used in each plane $P_k(R)$ (Fig. 1). Let $\Delta_{k,m}(R)$ be the propagation direction in the plane $P_k(R)$ characterized by the angle θ_m with the z-axis, θ_m being arbitrarily chosen in the range $[-\pi/2, \pi/2]$ $(m = -N_\theta, \ldots, -1, 1, \ldots, N_\theta)$. $2N_\theta$ angles $\Delta\theta_m$ which are divided into two equal parts by $\Delta_{k,m}(R)$ are defined by

$$\Delta\theta_1 = 2\theta_1$$

$$\Delta\theta_m = 2[\theta_m - (\theta_{m-1} + 0.5\Delta\theta_{m-1})], \quad m = 2, 3, \ldots, N_\theta - 1$$

$$\Delta\theta_m = \pi/2 - (\theta_{m-1} + 0.5\Delta\theta_{m-1}), \quad m = N_\theta. \tag{18}$$

$\Delta\theta_m$ $(m = -1, -2, \ldots, -N_\theta)$ is written in a similar manner.

A discrete solid angle $\Delta\Omega_{k,m}(R)$ $[\Delta\Phi_k(R), \Delta\theta_m]$ is then associated to each discrete direction $\Delta_{k,m}(R)$. N_r and N_θ are large enough to assume that the mean intensity in the discrete solid angle is correctly represented by the intensity in the direction $\Delta_{k,m}(R)$. The propagation direction $\Delta_{k,m}(R)$ is characterized by a unit vector in the plane P_k

$$\mathbf{u}(\theta) = \mathbf{e}_y \sin\theta + \mathbf{e}_z \cos\theta. \tag{19}$$

The definition of the discrete direction $\Delta_{k,m}(R)$ related to point S_0 of the external cylinder can be generalized to a current point M of an internal grid circle $(y_i, r_{k'})$, these directions are called $\Delta_{k,m}(r_{k'})$ $(k = 0, 1, \ldots, k')$. The plane containing M and the tangent to the cylinder r_k is quoted $\Pi_k(r_{k'})$ $(k = 0, 1, \ldots, k')$. The angle between the planes $\Pi_0(r_{k'})$ and $\Pi_k(r_{k'})$ is called $\Phi_k(r_{k'})$ and is given by (Fig. 2)

$$\Phi_k(r_{k'}) = \sin^{-1}(r_k/r_{k'}) \quad (k = 0, 1, \ldots, k'). \tag{20}$$

The angles $\Delta\Phi_k(r_{k'})$ are defined, by analogy with $\Delta\Phi_k(R)$, by the recurrence relations

$$\Delta\Phi_0(r_{k'}) = \Phi_1(r_{k'})$$

$$\Delta\Phi_k(r_{k'}) = 2[\Phi_k(r_{k'}) - \Phi_{(k-1)}(r_{k'})] - \Delta\Phi_{(k-1)}(r_{k'}), \quad k = 1, 2, \ldots, k'. \tag{21}$$

The discrete propagation directions $\Delta_{k,m}(r_{k'})$ at point $M(y_i, r_{k'})$ are then characterized by the angles $\Phi_k(r_{k'})$ and θ_m previously defined.

It is worth noting that in this model, the number $(k'+1)$ of Φ discrete values increases with $r_{k'}$; this fact is consistent with the decrease of the radiative flux $q_\nu(r)$ when r decreases. On the other hand, the intensity field in the $(k'+1)$ planes $\Pi_k(r_{k'})$ $(k = 0, 1, \ldots, k')$ is strictly identical to that in the plane $P_k(R)$ defined from the wall point S_0. Calculations of the radiative intensities are then only carried out in the N_r planes $P_k(R)$ $(k = 0, 1, \ldots, N_r - 1)$. Only the intensities calculated in the planes $P_k(R)$ $(k = 0, 1, \ldots, k')$ must be considered for calculations at the point $M(y_i, r_{k'})$. The intensities are calculated at all the grid points of a plane $P_k(R)$ for θ discrete values in the range $[-\pi/2, \pi/2]$; the intensity at point M in a direction $\mathbf{u}$ characterized by a value of θ outside this range is equal to that calculated at the symmetrical point M_s in the symmetrical direction $\mathbf{u}_s$ characterized by $(\pi - \theta)$ (Fig. 1). Equation (3) is written as

$$P(M) = -\sum_{\text{spectrum}} \sum_{k=0}^{k'} \sum_{m=-N_\theta}^{N_\theta} (2-\delta_{0k}) \times \left\{ \left[\frac{\partial \bar{I}_\nu(M, \Phi_k(r_{k'}), \theta_m)}{\partial y} + \frac{\partial \bar{I}_\nu(M_s, \Phi_k(r_{k'}), \theta_m)}{\partial y} \right] \times \int_{\Delta\Phi_k(r_{k'})} \int_{\Delta\theta_m} \sin\theta\cos\theta \, d\theta \, d\Phi + \left[\frac{\partial \bar{I}_\nu(M, \Phi_k(r_{k'}), \theta_m)}{\partial z} - \frac{\partial \bar{I}_\nu(M_s, \Phi_k(r_{k'}), \theta_m)}{\partial z} \right] \times \int_{\Delta\Phi_k(r_{k'})} \int_{\Delta\theta_m} \cos^2\theta \, d\theta \, d\Phi \right\} \tag{22}$$

where δ is the Kronecker symbol. Equation (5) is similarly written

$$q_{i\nu}(S) = \sum_{k=0}^{k'} \sum_{m=-N_\theta}^{N_\theta} (2-\delta_{0k}) \bar{I}_{i\nu}[S, \Phi_k(R), \theta_m] \times \int_{\Delta\Phi_k(R)} \int_{\Delta\theta_m} \cos\Phi\cos^2\theta \, d\theta \, d\Phi. \tag{23}$$

2.3.2. *Radiative intensity field.* In the following, subscript ν is left off for the sake of clarity. In a non-correlated approach, the spectral correlation between transmissivity and radiative intensity is omitted; equation (2) can be written as

$$\bar{I}^*(l,\mathbf{u}) = \bar{\tau}\bar{I}^*(0,\mathbf{u}) + (1-\bar{\tau})I_b(T) \quad (24)$$

where superscript * designates non-correlated quantities. The non-correlated intensities at all the grid points of plane P_k in the direction $\mathbf{u}(\theta)$ can be calculated step by step from this equation.

The intensity $\bar{I}^*(M,\mathbf{u})$ at a grid point M (Fig. 1) is composed of the transmitted part of the intensity $\bar{I}^*(M',\mathbf{u})$ at the non-grid point M' and of the emitted intensity by the column element between M' and M. The intensity $\bar{I}^*(M',\mathbf{u})$ at the non-grid point M' is obtained from an interpolation between the intensities at the neighbouring grid points K and J (Fig. 1); finally we obtain

$$\bar{I}^*(M,\mathbf{u}) = \bar{\tau}(MM')[f\bar{I}^*(K,\mathbf{u}) + (1-f)\bar{I}^*(J,\mathbf{u})] + [1-\bar{\tau}(MM')]I_b(MM'). \quad (25)$$

In this equation, the transmissivity $\bar{\tau}(MM')$ and the blackbody intensity $I_b(MM')$ are calculated with the averaged temperature, pressure and concentration of the column MM'; the coefficient f is given by

$$f = \Delta z \tan(\theta)/\Delta y \quad (26)$$

where Δy and Δz are the axial and transverse local steps in the plane P_k (Fig. 1). Equations (25) and (26) are only suitable for $0 \leqslant \theta \leqslant \tan^{-1}(\Delta y/\Delta z)$. Similar equations can be written for other θ ranges and for the wall grid points.

The non-correlated intensities at the grid points of line j are expressed vs the unknown wall leaving intensities from those of the line $j-1$; point (i,j) on line j is treated after point $(i-1,j)$ for $\theta \geqslant 0$ and before it for $\theta < 0$. For black walls, the wall leaving intensities are equal to the blackbody ones; the scheme is then explicit. Otherwise, the following procedure is used. The non-correlated intensity at any grid point $M(i,j)$ can be written as a function of the wall leaving intensities (Section 2.1)

$$\bar{I}^*(M,\mathbf{u}) = \sum_{S=1}^{N_w} \bar{a}_s^*(M,\mathbf{u})\bar{I}_{ls}(\mathbf{u}) + \bar{G}^*(M,\mathbf{u}) \quad (27)$$

where N_w is the number of discretized wall points; $\bar{a}_s^*(M,\mathbf{u})$ a coefficient related to the contribution of the intensity $\bar{I}_{ls}$ leaving a wall point S and $\bar{G}^*(M,\mathbf{u})$ the contribution of the medium emission. These coefficients are calculated step by step from formulas similar to equation (25). The initial boundary values of these coefficients are given by

$$\bar{a}_s^*(S',\mathbf{u}) = \begin{cases} 1, \text{ if } S \text{ and } S' \text{ designate the same point} \\ 0, \text{ if } S \text{ and } S' \text{ are two different points} \end{cases} \quad (28a)$$

$$\bar{G}^*(S,\mathbf{u}) = 0. \quad (28b)$$

This procedure is followed until the opposite walls are reached. The incident intensities on these walls are thus expressed in terms of the wall leaving intensities. Combining equations (5) and (6), we get a linear equation system. The resolution of this system gives the wall leaving intensities and then the non-correlated intensities at all the medium grid points.

2.3.3. *Spectral correlation model.* Radiative fluxes calculated from an RSNB model with the spectral resolution values $\Delta\nu = 25$ and $200\ \text{cm}^{-1}$ differ by about 15% [12]. The spectral resolution $\Delta\nu = 25\ \text{cm}^{-1}$ is chosen in the present study.

The exact correlated intensity at any grid point $M(i,j)$ of plane P_k is obtained without interpolation in the directions $0y$ and $0z$; e.g. the correlated intensity $\bar{I}(i,j,\mathbf{e}_z)$ at grid point $M(i,j)$ in the direction $0z$ is given by

$$\bar{I}(i,j,\mathbf{e}_z) = \bar{\tau}(i,j_s j)\bar{I}_l(i,j_s) + \sum_{j'=j_s}^{j-1} [\bar{\tau}(i,j'+1j) - \bar{\tau}(i,j'j)]I_b(i,j') + [1-\bar{\tau}(i,j)]I_b(i,j) \quad (29)$$

where (i,j_s) denotes a wall grid point S; $\bar{\tau}(i,j'j)$ is the correlated transmissivity of adjacent elements from $M'(i,j')$ to $M(i,j)$; it is calculated from equations (7) and (10)–(12); $\bar{I}_l(i,j_s)$ is the intensity leaving the point $S(i,j_s)$. It appears that the exact correlated intensity $\bar{I}(i,j,\mathbf{e}_z)$ at grid point $M(i,j)$ cannot be obtained from the correlated intensity $\bar{I}(i,j-1,\mathbf{e}_z)$ at the adjacent grid point $J(i,j-1)$; all the intermediate transmissivities $\bar{\tau}(i,j'j)$ must be calculated and stored to make such a correlated calculation. It is time consuming to do it for all discrete directions and grid points. On the contrary, the calculation of non-correlated intensities, established in the previous section, is relatively easy.

We define a corrective factor $C(M,\mathbf{u})$ for the grid point M and for the direction $\mathbf{u}(\theta)$, called the correlation coefficient

$$C(M,\mathbf{u}) = \frac{\bar{I}(M,\mathbf{u})}{\bar{I}^*(M,\mathbf{u})} \quad (30)$$

which will be modelled in this section. A planar geometry is first considered in order to validate this model with an exact calculation. In the case of a medium between two parallel infinite walls (Fig. 3), the non-correlated and correlated calculations have been carried out for all the directions, different wave number ranges, different temperature fields and different optical thicknesses. It appears that $C(M,\mathbf{u})$ is well approximated in the range $[0°, 70°]$ by the ellipse correlation coefficient $C_e(M,\mathbf{u})$ (Figs. 4 and 5)

$$C_e(M,\mathbf{u}) = [(C_1\cos\theta)^2 + (C_2\sin\theta)^2]^{1/2} \quad (31)$$

where C_1 and C_2 are two parameters calculated from the exact correlation coefficients in the directions characterized by $\theta = 0°$ and $70°$. The difference between

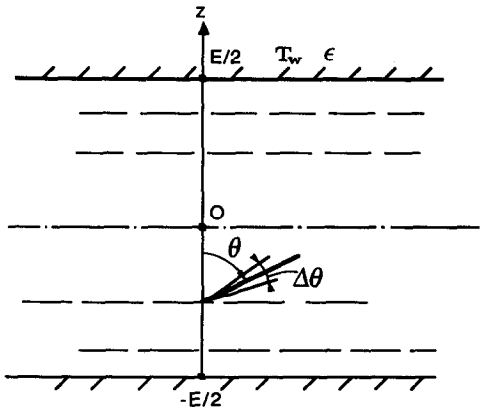

FIG. 3. Planar medium between two parallel walls.

the exact and ellipse correlation coefficients is smaller than 1% in the range [0°, 70°]. When θ tends to 90°, the column length increases, the medium becomes thick and isothermal in this direction. The correlation phenomena tend to disappear and $C(M, \mathbf{u})$ tends to 1.

For a two-dimensional axisymmetric system, an ellipse correlation coefficient $C_e(M, \mathbf{u})$ is calculated from the exact correlation coefficients in the directions

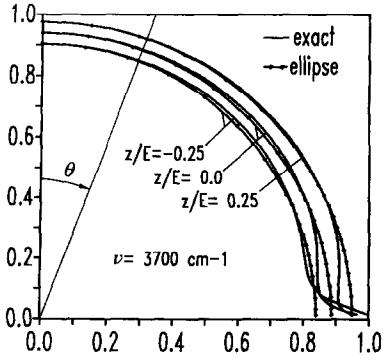

FIG. 4. Variations of the correlation coefficient C with θ in the case of pure water vapour between two parallel walls (the wall conditions and the medium temperature distribution are specified in Fig. 6(b).

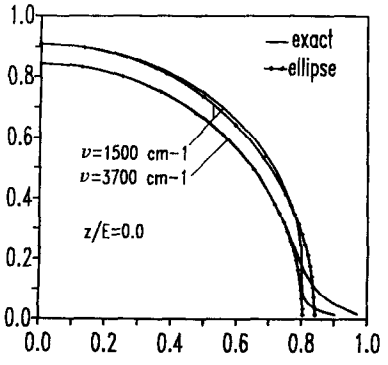

FIG. 5. Variations of the correlation coefficient C with θ in the case of a H_2O–N_2 mixture between two parallel walls ($E = 60$ cm, $T_w = 800$ K, $\varepsilon = 0.8$, $x_{H_2O} = 0.15$, $x_{N_2} = 0.85$, temperature field is given by $T(y) = 800 + 1200(1 - 2|z|/E)$).

$0y$ and $0z$ for each plane P_k. It is given at any grid point M of the plane P_k for any direction $\theta \geqslant 0°$ by

$$C_e(M, \mathbf{u}) = [(C(M, \mathbf{e}_z)\cos\theta)^2 + (C(M, \mathbf{e}_y)\sin\theta)^2]^{1/2} \quad (32a)$$

and for $\theta \leqslant 0°$ by

$$C_e(M, \mathbf{u}) = [(C(M, \mathbf{e}_z)\cos\theta)^2 + (C(M, -\mathbf{e}_y)\sin\theta)^2]^{1/2} \quad (32b)$$

where $C(M, \mathbf{e}_i)$ is the exact correlation coefficient for the direction $\mathbf{e}_i$. The validity of this model is discussed in Section 3.

3. RESULTS

3.1. *Planar geometry*

Calculations have been carried out in the case of water vapor between two isothermal parallel walls (Fig. 3) in order to validate the radiative transfer model. Results are compared to those of an exact correlated calculation using the RSNB model and the CG approximation for the same system [10]. Various optical thicknesses of the medium characterized by the distance E between the walls have been considered. Wall emissivity is assumed to be constant.

Four different models are used to calculate the radiative dissipation distribution P: (i) the exact correlated model of ref. [10]; (ii) the present correlated model for all the discrete directions; (iii) the ellipse correlated model; (iv) the non-correlated model. Results from these models are shown in Figs. 6(a)–(d). The radiative dissipation P obtained with model (ii) is in good agreement with that of model (i). In the case of wall emissivity greater than 0.5, differences between these two models are lower than 5% in the centre region, and smaller in the near wall region. In the case of reflecting walls ($\varepsilon = 0.01$), these differences are smaller than 10%.

No significant difference appears between the radiative dissipation P issued from model (ii) and the ellipse correlated model. The lack of validity of the ellipse correlated model in the θ range [70°, 90°] has no sensitive influence on the radiative dissipation. Two reasons explain this fact: (a) the difference between the ellipse and the exact correlation coefficients has not always the same sign in this range (Figs. 4 and 5); (b) the contribution of an elementary solid angle to the radiative dissipation decreases when θ increases up to 90°; the contribution of the range [70°, 90°] is generally lower than 4%.

The non-correlated model overpredicts the radiative dissipation P by about 20–30%. In the region near the wall the medium absorbs more radiative energy than it emits ($P > 0$), while in the centre region, emission is predominant ($P < 0$). The non-correlated model overestimates both absorption in the region near the wall and the medium emission in the centre region.

Wall radiative fluxes q_w calculated with the model

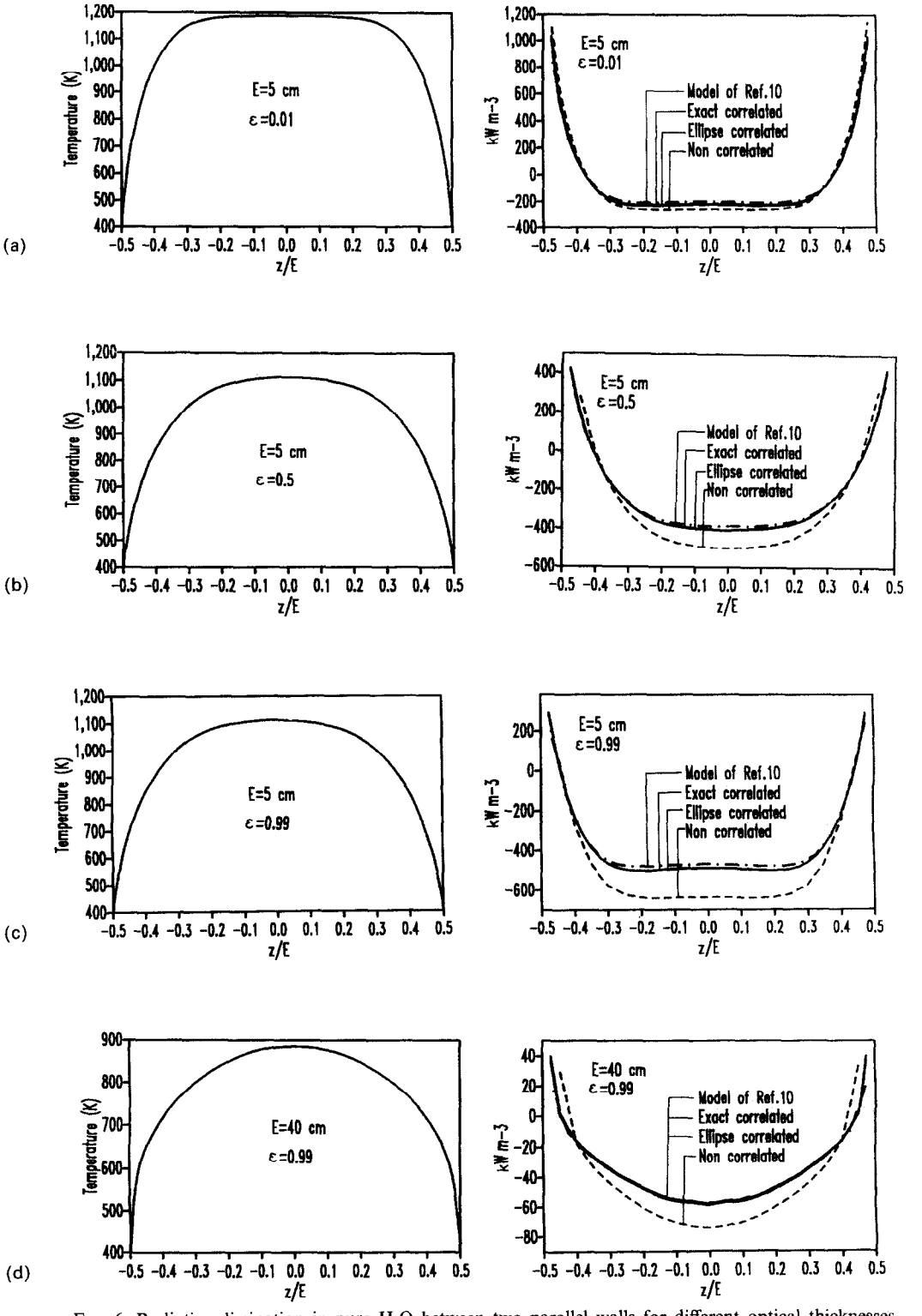

FIG. 6. Radiative dissipation in pure H_2O between two parallel walls for different optical thicknesses (characterized by E) and different values of wall emissivity. Temperature field is specified for each case.

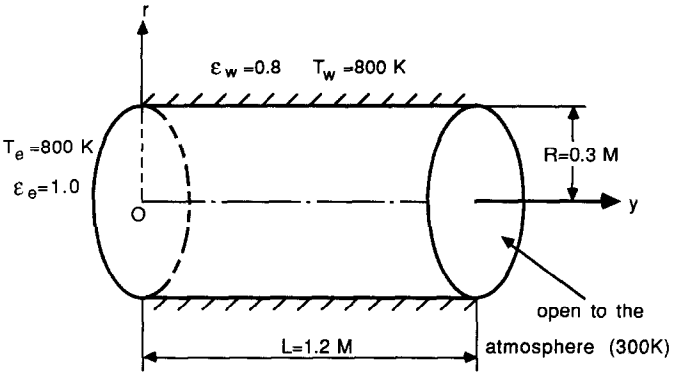

FIG. 7. Wall and geometrical conditions used in the cylinder calculations.

of ref. [10], with the ellipse correlated model and with the non-correlated model, are shown in Table 1. Differences between the two first models are smaller than the differences related to the radiative dissipation P. In fact, q_w is the integral of P over the range $-E/2 \leqslant y \leqslant E/2$; the non-correlated model overestimates the absolute value of P near the wall ($P > 0$) as in the centre region ($P < 0$). The non-correlated model also overestimates the radiative flux q_w by about 30%.

3.2. *Axisymmetric system*

The ellipse correlated and non-correlated models are used to predict the radiative transfer in an axisymmetric cylinder which is closed at the section $y = 0$ and open to the atmosphere at the section $y = L$. Wall conditions are reported in Fig. 7 (typical conditions of the combustion chamber of an aircraft engine). For practical computations, the section $y = L$ can be, in a first approximation, considered as a black wall. The medium is a H_2O–CO_2–CO–N_2–particle mixture. The particle spectral absorption coefficient is simplified from equation (13) [24]

$$K_\nu^p = 5.5\nu f_v \tag{33}$$

where ν is the wave number in cm^{-1} and K_ν^p is expressed in cm^{-1}. In the following, the total pressure is taken equal to 1 atm and the temperature distribution in the medium is assumed to be

$$T(r,y) = 800 + 1200(1 - r/R)(y/L). \tag{34}$$

Table 1. Wall radiative flux in the case of planar geometry (kW m^{-2}). Temperature distributions are specified in Fig. 6

Conditions	$E = 5$ cm $\varepsilon = 0.5$	$E = 5$ cm $\varepsilon = 0.99$	$E = 40$ cm $\varepsilon = 0.99$
Model of ref. [10]	5.113	8.675	6.803
Ellipse correlated model	5.189	8.824	6.533
Non-correlated model	6.270	11.41	7.639

The numerical results reported in this section are obtained with $(N_r, N_y, N_\theta) = (11, 12, 10)$.

The radiative flux at the lateral wall calculated with the exact and the ellipse correlated models are compared in order to validate the latter in the case of a homogeneous H_2O–N_2 mixture. Results show that the ellipse and the exact correlated models are in good agreement (Fig. 8(a)). This agreement is also obtained in the case of larger optical thicknesses (Fig. 8(b)). Important overestimations of the radiative flux by the non-correlated model are observed in the two cases. The overestimation of the q_w peak value reaches 90% in the case $x_{H_2O} = 0.15$ and 40% in the case $x_{H_2O} = 0.50$.

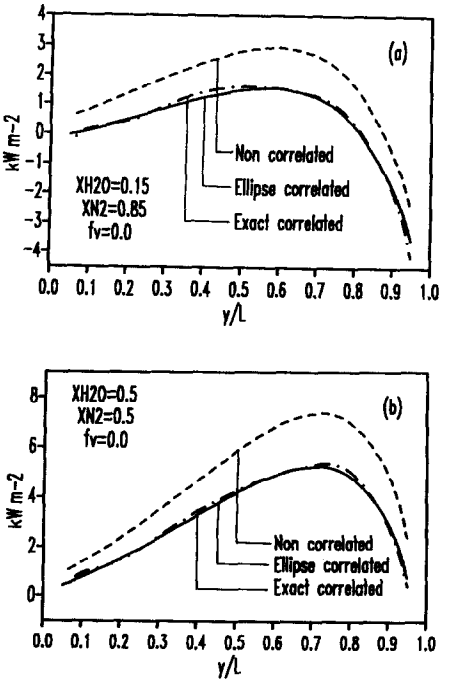

FIG. 8. Lateral wall radiative flux for an axisymmetric cylinder containing homogeneous H_2O–N_2 mixtures.

Radiative fluxes at the walls $y = 0, L$ and $r = R$ are computed with the ellipse correlated and the non-correlated models in the case of an inhomogeneous and non-isothermal H_2O–CO_2–CO–N_2 gas mixture (Fig. 9). The molar fraction distributions are given by

$$x_{H_2O} = 0.05\left[1-2\left(\frac{y}{L}-0.5\right)^2\right]\left(2-\frac{r}{R}\right)$$

$$x_{CO_2} = 0.04\left[1-3\left(\frac{y}{L}-0.5\right)^2\right]\left(2.5-\frac{r}{R}\right)$$

$$x_{CO} = 0.025\left[1-\frac{16}{9}\left(\frac{y}{L}-0.25\right)^2\right]\left(1.5-\frac{r}{R}\right)$$

$$x_{N_2} = 1-x_{H_2O}-x_{CO_2}-x_{CO}. \quad (35)$$

The non-correlated model predicts a positive value of q_w for the wall $y = 0$, while the ellipse correlated one predicts a negative value (see equation (4) for the sign of q_w). This qualitative disagreement is explained by the large discrepancies between the non-correlated and the correlated emissivities of the axis column lying from $y = 0$ to L (Fig. 10); the flux emitted by the gas, and then the absorbed fraction by the wall $y = 0$ are overestimated in the non-correlated approach; this results in the change of sign of q_w. The absolute overestimation of q_w by the non-correlated model is practically identical for all the walls.

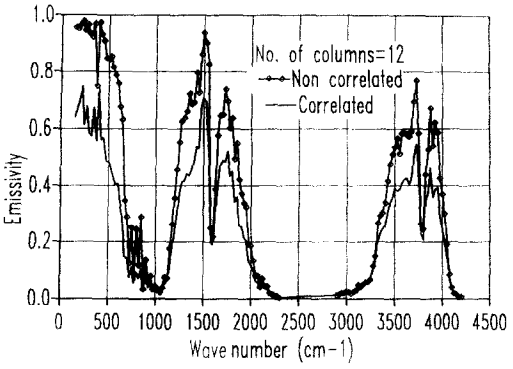

FIG. 10. Correlated and non-correlated emissivities of the gas mixture column lying from $y = 0$ to L: $x_{H_2O} = 0.15$; $x_{N_2} = 0.85$; $f_v = 0$.

The radiative dissipation P in the medium defined by equations (34) and (35) is plotted vs r/R and y/L in Fig. 11. Values of P obtained from the non-correlated model are larger than those obtained from the ellipse correlated model.

Radiative fluxes at the lateral wall are shown in Fig. 12 for gas–particle mixtures characterized by $x_{H_2O} = 0.15$, $x_{N_2} = 0.85$ and f_v varying from 0 to 10^{-4}. The absolute difference between radiative fluxes at the lateral wall calculated with the ellipse correlated and the non-correlated models is practically the same for different values of the particle volume fraction f_v. The lateral wall flux q_w increases when f_v increases up to 10^{-6}, and then decreases with f_v. This phenomenon is explained as follows: when f_v becomes large the medium becomes thick; radiation emitted by the hot

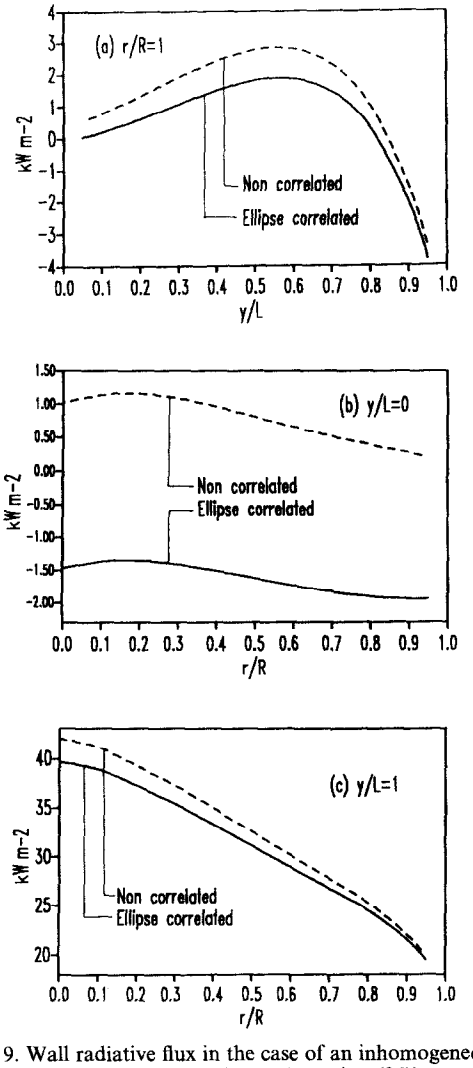

FIG. 9. Wall radiative flux in the case of an inhomogeneous H_2O–CO_2–CO–N_2 mixture (equation (35)).

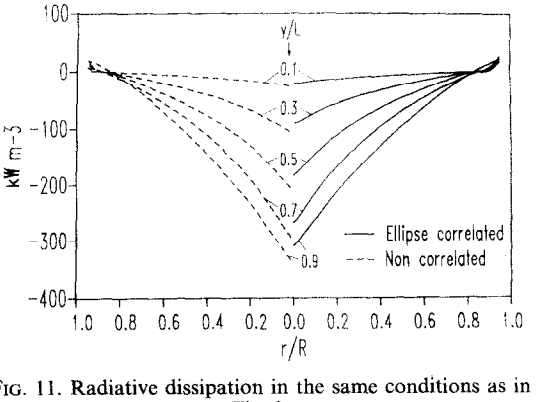

FIG. 11. Radiative dissipation in the same conditions as in Fig. 9.

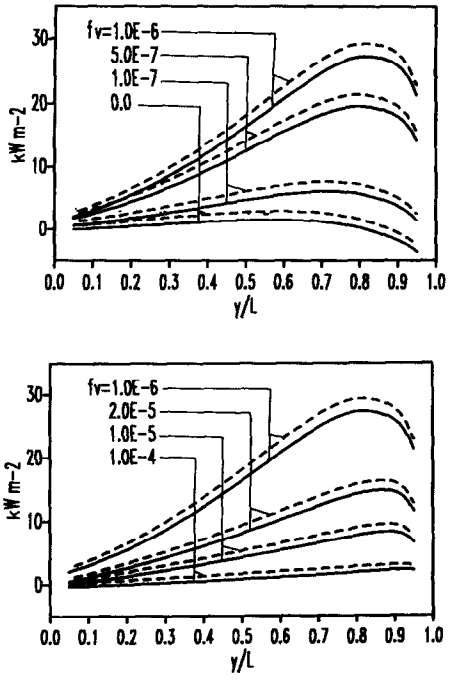

FIG. 12. Radiative flux at the lateral wall for different particle volume fractions (——, ellipse correlated model; – – – –, non-correlated model).

mixture in the centre region is not transmitted to the wall; the radiative flux q_w is then mainly due to radiation from the medium near the wall. The spectral ranges related to significant emission by particles and gas are practically separated. As a result, spectral correlated and non-correlated fluxes differ significantly even for high f_v values.

REFERENCES

1. R. Viskanta, Radiative heat transfer: interaction with conduction and convection and approximate methods in radiation, *Proc. 7th Int. Heat Transfer Conf.*, Vol. 1, p. 103, Munich (1982); see also: Radiative heat transfer, *Fortschr. Verf Tech.* **22,** 51 (1984).
2. S. S. Dua and P. Cheng, Multi-dimensional radiative transfer in non-isothermal cylindrical media with non-isothermal bounding walls, *Int. J. Heat Mass Transfer* **18,** 245 (1975).
3. M. P. Mengüc and R. Viskanta, Radiative transfer in axisymmetric, finite cylindrical enclosures, *J. Heat Transfer* **108,** 271 (1986).
4. M. P. Mengüc and R. Viskanta, Radiative transfer in three-dimensional rectangular enclosures containing inhomogeneous, anisotropically scattering media, *J. Quant. Spectrosc. Radiat. Transfer* **33,** 533 (1985).
5. D. K. Edwards and W. A. Menard, Comparison of models for correlation of total band absorption, *Appl. Optics* **3,** 621 (1964).
6. D. K. Edwards, Molecular gas band radiation. In *Advances in Heat Transfer*, Vol. 12, pp. 115–193. Academic Press, New York (1976).
7. C. L. Tien and J. E. Lowder, A correlation for total band absorption of radiative gases, *Int. J. Heat Mass Transfer* **9,** 698 (1966).
8. A. T. Wassel and D. K. Edwards, Molecular gas radiation in a laminar or turbulent pipe flow, *J. Heat Transfer* **98,** 101 (1976).
9. S. De Soto, Coupled radiation, conduction, and convection in entrance region flow, *Int. J. Heat Mass Transfer* **11,** 39 (1968).
10. A. Soufiani and J. Taine, Application of statistical narrow-band model to coupled radiation and convection at high temperature, *Int. J. Heat Mass Transfer* **30,** 437 (1987).
11. A. Soufiani, J. M. Hartmann and J. Taine, Validity of band-model calculations for CO_2 and H_2O applied to radiative properties and conductive–radiative transfer, *J. Quant. Spectrosc. Radiat. Transfer* **33,** 243 (1985).
12. A. Soufiani and J. Taine, Coupled convective and radiative transfer in strongly nonisothermal CO_2 and H_2O laminar flows, *Proc. 8th Int. Heat Transfer Conf.*, Vol. 2, pp. 791–796, San Francisco (1986).
13. W. L. Grosshandler, Radiative heat transfer in nonhomogeneous gases: a simplified approach, *Int. J. Heat Mass Transfer* **23,** 1447–1459 (1980).
14. W. L. Grosshandler and H. D. Nguyen, Application of the total transmittance nonhomogeneous radiation model to methane combustion, *J. Heat Transfer* **107,** 445 (1985).
15. R. M. Goody, *Atmospheric Radiation*, Chap. 4, pp. 122–170. Clarendon Press, Oxford (1964).
16. N. L. Godson, The evaluation of infrared radiative fluxes due to atmospheric water vapor, *Q. J. Meteor. Soc.* **79,** 367 (1953).
17. W. Malkmus, Random Lorentz band model with exponential-tailed S^{-1} line-intensity distribution, *J. Opt. Soc. Am.* **57,** 323 (1967).
18. C. B. Ludwig, W. Malkmus, J. E. Reardon and A. L. Thompson, *Handbook of Infrared Radiation from Combustion Gases*, NASA SP-3080. Scientific and Technical Information Office, Washington, DC (1973).
19. L. S. Bernstein, Band model parameters for the parallel bands of linear triatomic molecules—I. Theory, *J. Quant. Spectrosc. Radiat. Transfer* **23,** 157 (1980).
20. S. J. Young, Evaluation of nonisothermal band models for H_2O, *J. Quant. Spectrosc. Radiat. Transfer* **18,** 29 (1977).
21. J. M. Hartmann, R. Levi Di Leon and J. Taine, Line by line and narrow band statistical model calculations for H_2O, *J. Quant. Spectrosc. Radiat. Transfer* **32,** 119 (1984).
22. S. J. Young, Nonisothermal band model theory, *J. Quant. Spectrosc. Radiat. Transfer* **18,** 1 (1977).
23. R. Levi Di Leon and J. Taine, A fictive gas-method for accurate computations of low-resolution IR gas transmissivities: application to the 4.3 μm CO_2 band, *Revue Phys. Appliquée* **21,** 825 (1986).
24. R. O. Buckius and C. L. Tien, Infrared flame radiation, *Int. J. Heat Mass Transfer* **20,** 93 (1977).

TRANSFERTS RADIATIFS SPECTRALEMENT CORRELES ET NON CORRELES DANS UN SYSTEME AXISYMETRIQUE DE DIMENSIONS FINIES CONTENANT UN MELANGE ABSORBANT ET EMETTEUR GAZ REEL-PARTICULES

Résumé—On étudie le transfert radiatif dans une enceinte axisymétrique finie contenant un mélange de gaz et de particules anisotherme, hétérogène, absorbant, emetteur mais non diffusant. Un modèle statistique aléatoire à bandes étroites et l'approximation de Curtis–Godson sont utilisés pour calculer les propriétés radiatives réelles du gaz. Les corrélations spectrales à haute résolution entre les transmittivités des différents éléments de colonne de la discrétisation supposés homogènes et isothermes sont traitées par un modèle utilisant une indicatrice elliptique qui est validé. Une méthode de directions discrétes est utilisée afin de résoudre la partie géométrique du transfert radiatif. En appliquant ce modèle à un milieu plan et à une géométrie axisymétrique finie, il a apparait que les corrélations spectrales modifient de façon significative (typiquement 30 à 50%) le flux radiatif ainsi que la dissipation radiative au sein du milieu dans des systèmes concrets. Les modèles non corrélés peuvent aboutir à des prédictions qualitatives erronées (par exemple, le signe du flux radiatif peut être inversé).

DER SPEKTRALABHÄNGIGE UND UNABHÄNGIGE STRAHLUNGSAUSTAUSCH IN EINEM FINITEN ACHSENSYMMETRISCHEN SYSTEM, DAS EIN ABSORBIERENDES UND EMITTIERENDES GEMISCH REALER GASTEILCHEN ENTHÄLT

Zusammenfassung—Der Strahlungsaustausch in einem finiten achsensymmetrischen Bereich wurde für ein nicht-isothermes, inhomogenes, absorbierendes und emittierendes aber nichtstreuendes Gemisch aus Gasteilchen untersucht. Zur Berechnung des Strahlungsverhaltens eines realen Gases wird die Curtis–Godson-Näherung benutzt. Hochauflösende spektrale Beziehungen zwischen den Durchlässigkeiten von homogenen und isothermen diskretisierenden Elementen werden mit einem Modell behandelt, das sich auf Ellipsenbeziehungen stützt und validiert wurde. Eine Richtungsdiskretisierungs-Methode wird benutzt, um den geometrischen Teil des Strahlungsaustauschproblems zu lösen. Übertragungen auf ebene und finite achsensymmetrische Geometrien zeigen, daß die spektralen Zusammenhänge den Strahlungsfluß und die Strahlungsverteilung signifikant verändern—typisch im Bereich 30–50%. Nichtkorrelierende Modelle können zu qualitativ ungenauen Vorhersagen führen (z.B. Vorzeichenumkehr beim Strahlungsfluß).

СПЕКТРАЛЬНОЕ КОРРЕЛИРОВАННОЕ И НЕКОРРЕЛИРОВАННОЕ РАСПРОСТРАНЕНИЕ ИЗЛУЧЕНИЯ В КОНЕЧНОЙ ОСЕСИММЕТРИЧНОЙ СИСТЕМЕ, СОДЕРЖАЩЕЙ ПОГЛОЩАЮЩУЮ И ИЗЛУЧАЮЩУЮ СМЕСЬ РЕАЛЬНОГО ГАЗА И ЧАСТИЦ

Аннотация—Исследуется распространение излучения в конечномерной осесимметричной полости, содержащей неизотермическую, неоднородную, поглощающую и излучающую, но не рассеивающую смесь газа и частиц. Для расчета излучающих свойств реального газа используется хаотическая статистическая узкополосная модель и приближение Кертиса–Годсона. Спектральные корреляции высокого разрешения между коэффициентами пропускания одородных и изотермических элементов разделительной колонки обрабатываются при помощи эллиптической корреляционной модели. Для решения геометрической части задачи распространения излучения применяется метод дискретных направлений. В случае плоских и конечномерных осесимметричных геометрий показано, что спектральные корреляции значительно изменяют, в среднем на 30–50%, величину потока излучения и его рассеяние в практических системах. Нескоррелированные модели могут дать неточные качественные результаты (например, знак потока излучения может оказаться противоположным).